Metastatic melanoma: clinicopathologic features and overall survival comparison

Selin Kestel[1 ✉], Feriha Pınar Uyar Göçün[1,2], Betül Öğüt[1,2], Özlem Erdem[1,2]

[1]*Department of Pathology, Faculty of Medicine, Gazi University, Ankara, Turkey.* [2]*Gazi University Hospital, Ankara, Turkey.*

Abstract

Introduction: Five-year survival for melanoma with distant metastasis has been reported as 25%. This study evaluates the relationship between known and uncertain clinicopathologic parameters and overall survival (OS) for metastatic melanoma patients.
Methods: Metastatic melanoma cases (n = 122, 45 female, 77 male) that were metastatic at the time of diagnosis or referred for molecular pathological analysis were included. Survival was analyzed using the Kaplan−Meier method with comparisons performed by the log-rank test.
Results: The mean age of diagnosis at the time of metastasis was 56 years (range 19−89). The 1-year, 2-year, and 5-year OS rates were 44%, 27%, and 17%, respectively. Cox multiple regression analysis identified the following as independent poor prognostic factors for OS: perivascular pseudorosette formation (hazard ratio [HR]: 12.821, p = 0.045), lung compared to skin and subcutaneous soft tissue and to lymph node, specific cytologic features such as clear cytoplasm (p = 0.043), and hyperchromatic nuclei (HR: 98.605, p = 0.005) compared to vesicular chromatin pattern. At the end of the study, 26 (21%) of the patients were alive, and 96 (79%) were deceased.
Conclusions: In conclusion, perivascular pseudorosette formation, first described as a case report in primary and metastatic melanoma, may represent a new prognostic and diagnostic histopathological finding for metastatic melanoma.

Keywords: metastatic melanoma, histopathology, overall survival, perivascular pseudorosette, dermatopathology

Introduction

According to the United States 2022 cancer statistics, melanoma is the fifth most common malignancy in males and females (1). The rising incidence rate per year is approximately 3% in melanoma, and melanoma is among the most rapidly increasing malignancies concerning its incidence (2, 3). According to the Surveillance, Epidemiology, and End Result (SEER) Program database, the 1-year, 2-year, and 5-year survival rates for melanoma with distant metastasis are 48%, 36%, and 25%, respectively (4). Melanoma can metastasize both hematogenous and lymphatic routes with varying proportions. Based on clinical and radiological findings, melanoma can metastasize to every organ. The reported metastatic site ratios for melanoma are 10 to 60% for the skin, 10 to 40% for the lungs, 5 to 35% for distant lymph nodes, 15 to 20% for the liver, 5 to 20% for the central nervous system (CNS), 5 to 20% for bones, 1 to 10% for the gastrointestinal system, 1 to 10% for the adrenal glands, < 5% for the pleura, < 5% for the pancreas, < 1% for the heart, < 1% for the kidneys, < 1% for the thyroid, and < 1% for the uterus (5). This study sought to identify or confirm any new or suggested histopathological predictors related to overall survival (OS).

Methods

This study included 122 metastatic melanoma cases (45 females and 77 males) that were metastatic at the time of diagnosis or referred for molecular pathological analysis between January 2008 and March 2020. The last follow-up was determined as April 2021. The clinicopathological and outcome data were acquired from electronic medical records. The OS time was calculated as the time from diagnosis to death from any cause or last follow-up (censored). The following histopathological parameters were evaluated from archival slides: pigmentation, necrosis, perivascular pseudorosette, tumor-infiltrating lymphocytes (TILs), pleomorphism, cell type, cytoplasmic and nuclear features, and mitotic count.

Pigmentation was evaluated as either absent or present if there was any amount of melanin. Necrosis was evaluated as present even if this was in a single focus. Perivascular pseudorosette formation was evaluated as present even in a single focus of melanocytes arranged radially around blood vessels with a perivascular acellular zone. TIL was assessed similar to primary cutaneous melanoma (6). However, TIL was considered present regardless of intensity. Pleomorphism was assessed as low or high according to the variation in size and shape of nuclei, prominence, and size of nucleoli. Cytoplasmic staining with hematoxylin and eosin (H&E) was evaluated according to the predominance and the intensity of eosinophilic staining and accompanying clear cells as eosinophilic-clear, clear, eosinophilic, pale eosinophilic, or pale eosinophilic-clear. Heavily pigmented cases were not included in this cytoplasmic assessment. Nuclear hematoxylin staining was evaluated as hyperchromatic when the nuclei were dark hyperchromatic, vesicular when the nucleoli were prominent and the nuclei were pale, and neuroendocrine-like when the chromatin had a salt-and-pepper appearance reminiscent of neuroendocrine neoplasm.

The use of immunohistochemistry (i.e., S100, Melan-A, and HMB-45) for diagnosis and *BRAF* V600 mutation status (previously performed with real-time polymerase chain reaction [RT-PCR] or next-generation sequencing [NGS]) were noted. Immunostainings were performed with external controls and accepted as positive or immunoreactive when staining was either rare, scattered/

✉ Corresponding author: selinkestel@gmail.com

focal/diffuse and weak/strong, or cytoplasmic (for Melan-A and HMB-45), cytoplasmic and/or nuclear (for S100). RT-PCR for *BRAF* V600 mutation was tested using either the AmoyDx BRAF V600 Mutations Detection Kit (Amoy Diagnostics Co., Xiamen, China) or Cobas® BRAF V600 mutation kit (Roche, Pleasanton, CA, USA). NGS with Qiagen GeneReader workflows (Qiagen, Hilden, Germany), according to the manufacturer's protocol, was performed by isolating deoxyribonucleic acid (DNA) from the biopsy specimens.

Survival analysis was calculated using the Kaplan–Meier method with SPSS version 23 (IBM Corp., Armonk, NY, USA). Differences between survival functions were analyzed by log-rank test. The statistically significant difference between groups was determined as $p < 0.05$. Cox (proportional hazards) multiple regression analysis was performed for covariates with a *p*-value of < 0.25 and continuous covariates. When more than one covariate

was highly correlated, one was integrated into the model to minimize covariates and increase the model's validity.

All procedures performed in this study were approved by the Institutional Review Board (IRB; reference number 357, May 22nd, 2020). Informed consent was waived due to the retrospective nature of this study.

Results

The patients and tumor characteristics are shown in Tables 1, 2, and 3. The mean follow-up time was 20.7 months (median 10, range 1–145). In our study, the calculated 1-year, 2-year, and 5-year OS probabilities were 44%, 27%, and 17%, respectively (Fig. 1A). The mean age of diagnosis at the time of metastasis was 56 ± 1.36 years (median 58, range 19–89). All patients ≤ 30 years old were

Table 1 | Univariate analysis of predictors for overall survival time (months) in metastatic melanoma, calculated from Kaplan–Meier analysis with comparisons performed with the log-rank test.

	n (% of total or % of total for category)	Deaths (% of total for subcategory)	Mean ± *SE* (95% CI) (months)	*p*
Overall survival	122 (100)	96 (79)	33.02 ± 4.94 (23.35–42.70)	
Sex	122 (100)			
Male	77 (63)	64 (83)	28.36 ± 5.48 (17.62–39.11)	0.316
Female	45 (37)	32 (71)	40.66 ± 9.10 (22.82–58.50)	
Age at diagnosis (years)	122 (100)			
‹ 58	59 (48)	45 (76)	41.0 ± 7.32 (26.65–55.35)	**0.047**
≥ 58	63 (52)	51 (81)	17.14 ± 3.32 (10.64–23.64)	
Age at diagnosis (years)	122 (100)			
0–30	5 (4)	5 (100)	9.4 ± 2.99 (3.53–15.27)[ab]	
31–60	65 (53)	47 (72)	43.72 ± 7.35 (29.31–58.13)[a]	**0.010**
› 60	52 (43)	44 (85)	15.43 ± 3.33 (8.90–21.95)[b]	
Site	120 (98)			
Lymph node	34 (28)	22 (65)	44.13 ± 8.30 (27.86–60.40)[c]	
CNS	31 (26)	29 (94)	15.65 ± 6.17 (3.56–27.74)[a]	
Skin / soft tissue	26 (22)	17 (65)	52.05 ± 12.80 (26.97–77.13)[cd]	
Liver	17 (14)	14 (82)	16.88 ± 6.08 (4.97–28.80)[ad]	**‹ 0.001**
Lung	10 (8)	10 (100)	11.70 ± 4.85 (2.20–21.20)[a]	
Bone marrow	1 (1)	1 (100)	5.0 ± 0.0 (5.0–5.0)[ad]	
Paranasal sinus	1 (1)	1 (100)	2.0 ± 0.0 (2.0–2.0)[ab]	
Biopsy procedure	122 (100)			
Incisional	34 (28)	29 (85)	15.27 ± 3.63 (8.17–22.38)	**0.050**
Excisional	88 (72)	67 (76)	38.02 ± 6.11 (26.04–50.00)	
BRAF V600 mutation	60 (49)			
Negative	37 (63)	25 (68)	40.03 ± 8.69 (22.99–57.06)	0.989
Positive	22 (37)	16 (73)	26.93 ± 6.11 (14.96–38.90)	
Perivascular pseudorosette	122 (100)			
Negative	58 (47)	40 (69)	46.29 ± 8.21 (30.21–62.37)	**0.003**
Positive	64 (53)	56 (88)	20.91 ± 5.32 (10.47–31.34)	
Mitotic count (/mm²)	122 (100)			
0–6	64 (52)	49 (77)	36.37 ± 6.97 (22.72–50.03)	0.282
› 6	58 (48)	47 (81)	29.02 ± 6.71 (16.06–42.34)	
TILs	85 (70)			
Absent	43 (51)	38 (88)	21.33 ± 6.38 (8.82–33.83)	0.339
Present	42 (49)	33 (79)	32.67 ± 8.47 (16.06–49.28)	
Cell type	122 (100)			
Epithelioid	59 (48)	44 (75)	39.29 ± 7.65 (24.30–54.27)	
Spindle	16 (13)	10 (63)	56.91 ± 16.96 (23.67–90.16)	0.060
Other	47 (39)	42 (89)	17.20 ± 3.99 (9.37–25.03)	
Cytoplasm	117 (96)			
Clear	4 (3)	4 (100)	13.25 ± 10.31 (0.00–33.45)[ab]	
Pale eosinophilic	17 (15)	15 (88)	9.77 ± 2.98 (3.92–15.61)[a]	
Eosinophilic	73 (62)	56 (77)	38.85 ± 6.66 (25.79–51.91)[bd]	**0.013**
Pale eosinophilic-clear	10 (9)	5 (50)	66.04 ± 21.77 (23.38–108.70)[cd]	
Eosinophilic-clear	13 (11)	12 (92)	14.85 ± 8.26 (0.00–31.01)[a]	
Nuclear chromatin	111 (91)			
Vesicular	82 (74)	63 (77)	37.95 ± 6.15 (25.89–50.01)[a]	
Hyperchromatic	25 (23)	19 (76)	20.48 ± 5.85 (9.01–31.94)[ab]	**0.018**
Neuroendocrine-like	4 (3)	4 (100)	4.25 ± 0.85 (2.58–5.92)[b]	

n = number, *SE* = standard error, CI = confidence interval, TILs = tumor-infiltrating lymphocytes.
The same letters mean there is no difference between groups.

Table 2 | Cox multiple regression for overall survival in metastatic melanoma cases.

			95% CI for HR*	
	p	HR	Lower	Upper
Model (overall)	**0.015**	–	–	–
Site	**0.046**			
Liver (ref: lung)	0.539			
CNS (ref: lung)	0.394			
Lymph node (ref: lung)	**0.047**	0.004	0.000	0.934
Skin and subcutaneous soft tissue (ref: lung)	**0.032**	0.004	0.000	0.632
Perivascular pseudorosette	**0.045**	12.821	1.060	155.089
Cytoplasmic staining	**0.043**			
Pale eosinophilic (ref: clear)	**0.033**	0.001	0.000	0.569
Eosinophilic (ref: clear)	**0.011**	0.000	0.000	0.151
Pale eosinophilic-clear (ref: clear)	**0.003**	0.000	0.000	0.008
Eosinophilic-clear (ref: clear)	**0.012**	0.001	0.000	0.205
Nuclear chromatin	**0.018**			
Hyperchromatic (ref: vesicular)	**0.005**	98.605	3.923	2,478.280
Neuroendocrine-like (ref: vesicular)	0.060			

HR = hazard ratio, CI = confidence interval, CNS = central nervous system, ref = reference.
*Statistical significance ($p < 0.05$).

Table 3 | Other molecular alterations identified by mutational testing in a subset of patients.

Age (years)	Sex	Biopsy site	Other mutation(s)	*BRAF* status	Method	Outcome/survival (at last follow-up)
64	M	Right neck, subcutaneous soft tissue	NRAS Exon 3 Q61R	Wild-type	NGS	Alive / 22 months
28	M	Brain	FBXW7 Exon 10 R505C MET Exon 2 S290F	*BRAF* Exon 15 V600E*	NGS	Death / 10 months
51	M	Lymph node	NRAS Exon 3 Q61K KIT Exon 13 N655K KIT Exon 10 M541L	Wild-type	NGS	Death / 24 months
54	M	Liver	KRAS Codon 12(Gly12Asp)	Wild-type	RT-PCR	Death / 1 month

M = male, NGS = next-generation sequencing, RT-PCR = real-time polymerase chain reaction.
*RT-PCR was negative for *BRAF* V600 mutation; however, NGS detected BRAF mutation.

deceased, with the poorest OS in this study ($p = 0.093$ for comparison with 31–60 years, $p = 0.778$ for comparison with > 60 years; Fig. 1B). Lung and CNS metastasis had a worse OS than lymph node ($p = 0.003$ for the lung, $p < 0.001$ for the CNS) and skin and subcutaneous soft tissue ($p = 0.023$ for the lung, $p = 0.004$ for the CNS; Table 1, Fig. 1C). Liver ($p = 0.022$), bone marrow ($p = 0.021$), and paranasal sinus metastasis ($p = 0.007$) had poor OS compared to lymph node metastasis. An excisional biopsy in metastatic melanoma cases was related to improved OS ($p = 0.050$). At the end of the study, 26 (21%) of the patients were alive, and 96 (79%) were deceased.

BRAF V600 mutation analysis was performed for 59 cases during the initial diagnosis of each case, and mutation was present in 22 (37%) tumor tissues, whereas 37 (63%) tumor tissues were negative for *BRAF* V600 mutation ($p = 0.989$). Mutation detection methods were mostly RT-PCR for *BRAF* V600 mutant ($n = 20$) and *BRAF* V600 mutation-negative ($n = 34$) cases. Mutation detection kits for *BRAF* V600 mutation-negative cases were AmoyDx in 21 cases and Cobas® in 13. NGS was the mutation detection method of choice for the additional three *BRAF*-wild type cases (Table 3). Mutation detection kits for *BRAF* V600 mutant cases were Cobas® in 12 cases and AmoyDx in eight. In one case, *BRAF* V600E mutation was detected via NGS at exon 15. However, this case was negative for *BRAF* V600 mutation with previously performed RT-PCR using the AmoyDx mutation detection kit (Table 3). In another case, only clinical information was available for *BRAF* mutation without subtyping whether it was V600 or not. There was no melanin pigment in 40 (33%) cases ($p = 0.937$). Necrosis was present in 84 (69%) cases ($p = 0.853$). Perivascular pseudorosette formation (Figs. 2, 3) was noticed in 64 (53%) metastatic melanoma cases and reduced OS significantly ($p = 0.003$; Fig. 1D).

The median number of mitoses was 6/mm² (range 0–36; $p = 282$). Cytoplasmic staining features (Figs. 2–4) with H&E were significantly associated with OS ($p = 0.013$; Fig. 1E). The most frequent cytoplasmic staining appearance was eosinophilic in 73 (62%) samples (Figs. 2B, 4D). Pale eosinophilic-clear staining had improved OS compared to clear ($p = 0.047$; Fig. 4C), pale eosinophilic ($p = 0.007$; Fig. 4E), and eosinophilic-clear (Figs. 4A, 4B) staining ($p = 0.013$). The most frequent nuclear appearance was vesicular (Figs. 4A, 4D) in 82 (74%) cases and was more associated with improved OS than rarely observed neuroendocrine-like nuclei (3%; $p = 0.018$; Fig. 1F). Pleomorphism ($p = 0.179$) and nucleolar prominence ($p = 0.370$) were not associated with OS. Different combinations of immunohistochemical stains were performed as part of the initial diagnostic evaluation. Positive immunoreactions were observed with S-100 in 45 cases ($n = 46$, $p = 0.043$), Melan-A/MART-1 in 50 cases ($n = 53$, $p = 0.197$), and HMB-45 in 78 cases ($n = 82$, $p = 0.441$). Combining these three stains resulted in no immunoreactivity for Melan-A/MART-1 in one case, for HMB-45 in two cases, and for HMB-45&Melan-A/MART-1 in another two cases. One case was immunoreactive for HMB-45 but not for S-100. OS was better in cases with S-100–positive staining compared to no immunoreactivity for S-100 ($p = 0.043$).

In this study, Cox multiple regression analysis indicated that lung compared to skin and subcutaneous soft tissue (HR: 0.004, $p = 0.032$) and lymph node (HR: 0.047, $p = 0.004$), and perivascular pseudorosette structure (HR: 12.821, $p = 0.045$) were independent poor prognostic factors for OS. In addition, specific cytologic features such as clear cytoplasm ($p = 0.043$) and hyperchromatic nuclei (HR: 98.605, $p = 0.005$) compared to vesicular chromatin patterns were associated with poor OS as an independent prognostic factors (Table 2).
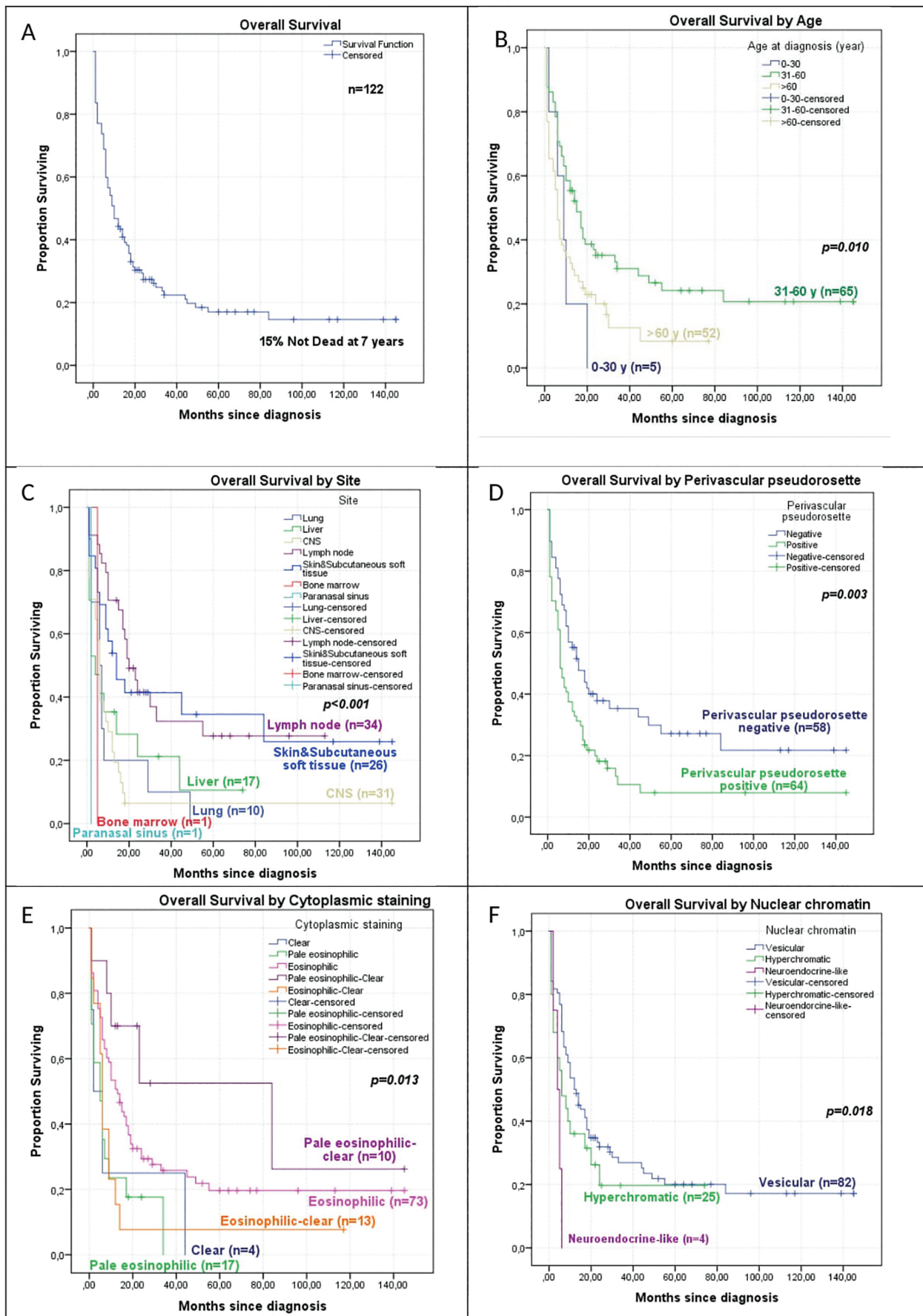
Figure 1 | Kaplan–Meier overall survival curves for metastatic melanoma (A) compared for tumor variables by age (B), site (C), perivascular pseudorosette (D), and cytoplasmic (E) and nuclear (F) staining patterns.
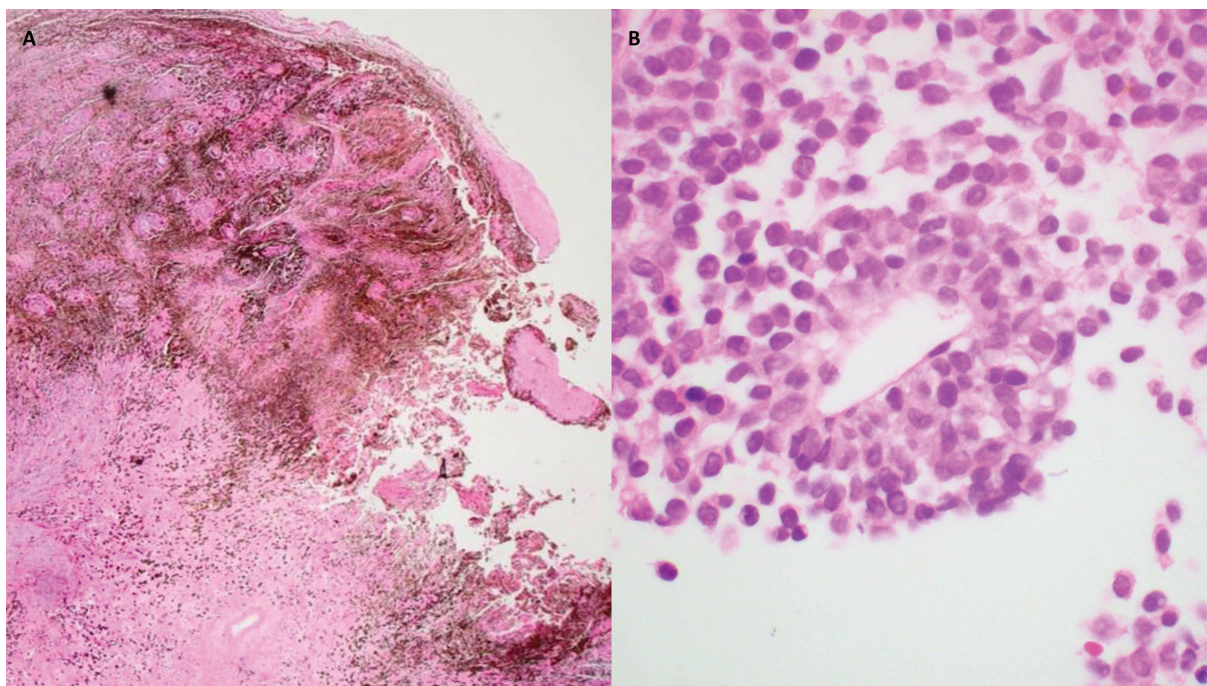
Figure 2 | (A) A 48-year-old male patient's mass located at the C7-T1 level demonstrates a highly vascularized and pigmented tumor exhibiting mainly perivascular arrangement. Necrosis accompanies neoplasia (H&E; 12.5×). The tumor cells are positive for S100 and Melan-A staining in a diffuse cytoplasmic pattern. (B) A 58-year-old female patient with a known melanoma diagnosis presents with subcutaneous metastasis to the right thigh. Needle biopsy shows monotonous small epithelioid cells, with eosinophilic cytoplasm and mostly hyperchromatic nuclei containing rare nucleoli, aligned radially around a thin-walled vessel, exhibiting angiotropism and reminiscent of perivascular pseudorosette. The tumor is positive for HMB-45 and SOX10 staining and harbors *BRAF* V600 mutation (H&E; 400×).
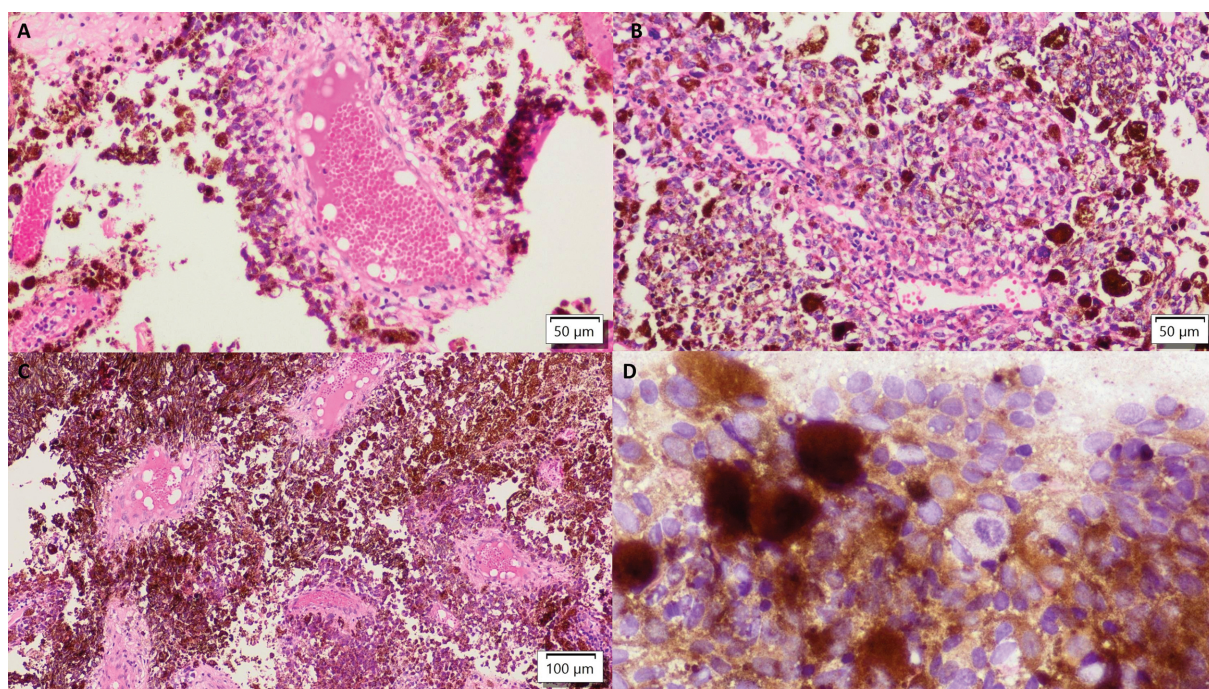

Figure 3 | A 71-year-old female patient's brain metastatic melanoma is comprised of highly pigmented spindle-shaped cells without nucleoli radially arranged around blood vessels with a perivascular acellular area (H&E; A 200×, C 100×). In some areas, lymphocytes surround blood vessels before malignant melanocytes in this case, and in some other brain metastatic melanoma cases (H&E; B 200×). The frozen sample exhibits large and pleomorphic malignant melanocytes with mitotic figures accompanying intense melanin pigmentation (H&E; D 400×).

Discussion

Various studies contain controversial clinicopathologic prognostic parameters for evaluating primary cutaneous melanoma. However, a comprehensive study by Xiao et al. (7) including 66,192 non-metastatic cutaneous malignant melanoma patients from the SEER program reported that age, sex, race, marital status, anatomic site, stage, depth, ulceration, mitoses, and treatment were prognostic factors for OS in univariate and multivariate Cox proportional hazards regression. In addition, solar elastosis and precursor lesions have been the main factors for classifying melanoma developmental pathways (3). *KIT*, *BRAF*, *NRAS*, and *NF1* mutations are also crucial for the molecular subtyping of melanoma (8). The mutation frequencies for cutaneous melanoma are 35 to 50% for *BRAF* V600 (9), 24% for *NRAS* (9), and 10% for *NF1* (10). *NRAS* mutation occurs the most frequently at codon Q61 (11). In desmoplastic melanoma, receptor tyrosine kinase gene amplifications (*EGFR*, *MET*, *ERBB2*) may be seen more frequently (12).
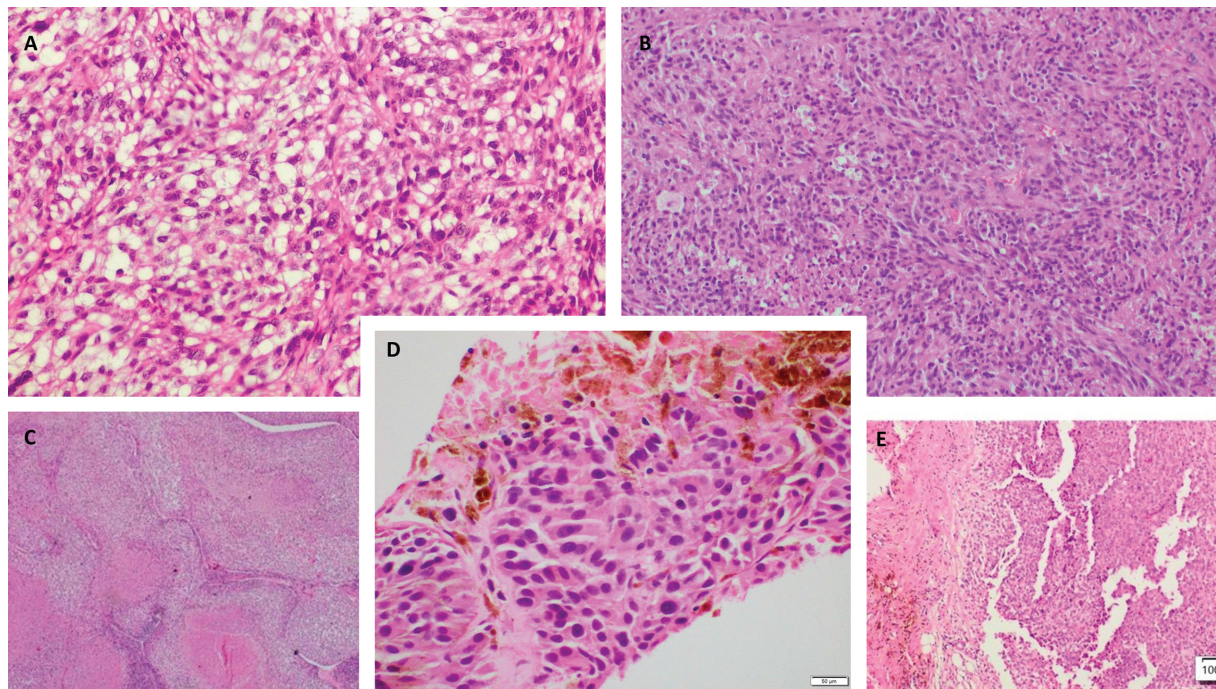
Figure 4 | These are mainly examples of cytoplasmic staining properties. (A) A 62-year-old female patient's mass from trunk subcutaneous soft tissue exhibits cells with cytoplasmic clearing and eosinophilia with vesicular nuclei (H&E; 200×). (B) A 28-year-old male patient with a melanoma diagnosis presents brain metastasis comprised of the spindle to epithelioid cells with cytoplasmic eosinophilia and rare clearing containing hyperchromatic nuclei. Metastatic melanocytes have mutations for *BRAF* exon 15 V600E, *FBXW7* exon 10 R505C, and *MET* exon 2 S290F (H&E; 200×). (C) An 80-year-old female patient's metastatic lymph node melanoma is composed of clear epithelioid to spindle cells forming islands with central necrosis (H&E; 40×). (D) A 63-year-old male patient presents with a lung mass. Needle biopsy reveals moderately pigmented necrotic metastatic melanoma composed of eosinophilic cells with vesicular nuclei. There is no *BRAF* V600 mutation with RT-PCR (H&E; 200×). (E) A 67-year-old male patient presents with neck region subcutaneous soft tissue metastatic melanoma consisting of epithelioid pale eosinophilic melanocytes (H&E; 100×).

BAP1 inactivation (8), *HRAS* mutations (8), translocations, and kinase fusions, including receptor tyrosine kinase genes such as *ALK*, *ROS1*, *NTRK1*, *NTRK3*, *RET*, and *MET*, may be seen more frequently in Spitz melanoma (13–16). *CCDN* (cyclin D1) and *KIT* mutations are more common than other subtypes in acral melanoma (17–19). For uveal melanoma, cellular features, tumor thickness, and the largest basal diameter are evaluated for grading and staging (2, 20). For conjunctival melanoma, cellular features are a predictive factor (21). There are also candidate poor prognostic features for OS in conjunctival melanoma, including ulceration, tumor thickness > 2 mm, and a mitotic count of > 1/mm² (21–23). In the head and neck region for mucosal melanoma, local infiltration of deep soft tissue, cartilage, and bone are becoming additional prognostic parameters (24). On the other hand, there are no Union for International Cancer Control (UICC) staging criteria for gastrointestinal melanoma (including anorectal melanoma) (12, 24). No consensus guidelines exist for staging vaginal, vulvar, male genitourinary, or urinary tract melanomas (25). In line with the data mentioned above and with the support of clinical, histopathological, epidemiological, and genomic observations, nine different pathways were described for melanoma development in the 2018 World Health Organization Classification of Melanoma (3, 12). When we evaluated metastatic melanoma, we tried to analyze the available clinical and histopathologic prognostic variables from an unknown primary perspective.

Sandru et al. (26) reported the metastatic sites as the brain in 27 (44%) patients, nonregional lymph nodes in 17 (27%) patients, the ovaries in one patient, subcutaneous soft tissue in 15%, the lungs in 13%, and the digestive tract in 13%. Taş et al. (27) reported 365 cutaneous melanoma patients with 189 early recurrences (within 18 months) and 176 late recurrences (more than 18 months later).

They reported that the lungs (43%) were the most common metastatic site, followed by bone (21%), the liver (21%), and the brain (15%). In our study, CNS metastasis (26%) was more frequent than in Taş et al.'s study (27), whereas lung metastasis (8%) was less common than in previous studies (26, 27). Although the study designs and case numbers differed, the relationship between OS and metastatic site is shared between this study and similar studies (26, 27). Complete surgical excision for the skin, subcutaneous soft tissue, and nonregional lymph node metastasis gave patients a 23% OS probability and a more favorable prognosis than other metastatic sites (28).

Melanoma can exhibit many different cytologic, structural, and stromal morphologic patterns and may mimic carcinoma, sarcoma, benign stromal tumors, lymphoma, plasmacytoma, and germ cell tumors (29). A rarely observed or overlooked stromal change in melanoma is pseudorosette formation or an angiocentric pattern (29, 30). Upadhyay Baskota et al. (30) recently reported that a peritheliomatous pattern characterized by a sheath of viable tumor cells closely surrounding a central blood vessel could help diagnose metastatic melanoma in cytology specimens. Rarely unclassified rosette-forming or Homer Wright–like rosette-forming primary, metastatic, or atypical melanocytic proliferations have been reported (31–34). Ishida et al. (35) described a case with perivascular pseudorosette formation in primary melanoma with lymph node metastasis. In that case, melanoma had a component of deeply localized melanocytes arranged radially around blood vessels with a perivascular acellular zone. In our study, perivascular pseudorosette formation with the same histopathologic description as the reported case was statistically significantly related to poor OS in univariate and Cox multiple regression analyses.

Malignant melanocytes have different migratory pathways to

leave the primary melanoma mass and invade local and distant regions (36). This plasticity of malignant melanocytes has been associated with their embryonic or stem cell–like cellular feature (37, 38). The primary metastatic mechanism for cancer cells is accepted as intravascular dissemination via lymphatic or blood vessels (39). On the other hand, Lugassy and Barnhill introduced extravascular migratory metastasis in melanoma (EVMM) almost two decades ago (40). Malignant melanocytes migrate without intravascular dissemination in EVMM. Angiotropism is described as the attachment of tumor cells to the abluminal surface of vessels. Then, malignant melanocytes migrate throughout the extravascular area using selective motility clues (41). Angiotropic malignant melanocytes are generally found on the invasive side of the tumor mass, and they have a close relation with endothelial cells, like a pericyte without intravasation (42). Thus, angiotropism provides pericytic mimicry to malignant melanocytes. In this way, melanoma cells can migrate throughout extravascular space (42).

Barnhill et al. (43) reported the relation of angiotropism to prognosis. That study compared 40 cases of metastatic primary cutaneous melanoma with 40 cases of non-metastatic primary cutaneous melanoma. They did not find a significant survival difference between angiotropic melanoma and cases without angiotropism. However, angiotropism was identified more frequently in metastatic melanoma cases ($p = 0.008$). Moreover, in all but one case there was no lymphovascular invasion in angiotropic metastatic melanoma cases. Another study revealed that angiotropism is a prognostic factor determining local and in-transit metastasis in primary melanoma (44). In primary cutaneous melanoma, the presence of angiotropism was found to be correlated with microscopic satellites (45). Although perivascular pseudorosette formation does not have the same appearance as angiotropism, melanocytes forming perivascular pseudorosettes were also determined to exhibit angiotropism (46). Thus the reduced OS in metastatic melanoma that formed perivascular pseudorosettes might represent an example of melanoma extravascular metastasis pathways.

Primary cutaneous, mucosal, and metastatic melanoma can contain glycogen-rich clear cells (47). In this study, all metastatic melanoma cases with clear cells ($n = 4$) were deceased by the end of the study. Nowak et al. (48) investigated 61 excisional biopsies of 58 malignant melanoma patients and 17 nevi from 10 patients for periodic acid–Schiff (PAS) stain positivity. They observed PAS positivity in all cases. Moreover, focal or diffuse, strong, diastase-sensitive PAS positivity was seen in nine (15%) of 61 melanoma cases. Seven of these cases were metastatic melanoma, and two of them were primary invasive malignant melanoma. The presence of glycogen was confirmed by transmission electron microscopy (48). One of our cases with eosinophilic cytoplasm accompanying clear vacuoles also had diastase-sensitive PAS positivity in lymph node metastatic melanoma.

Glycogen synthase kinase-3 (GSK-3) is a serine/threonine kinase involved in carcinogenesis alongside its initially discovered role in glycogen synthesis and accumulation (49). It has an opposite role in cancer development depending on the cellular context. Therefore, GSK-3 has been an attractive therapeutic target for many cancers, including melanoma. GSK-3 inhibition has resulted in population reduction in human melanoma cell lines, the apoptotic phenotype in some of them, dendritic process extension in melanoma cells similar to differentiated melanocytes, and loss of PAX3 expression in human melanoma cell lines (50). GSK-3 inhibitors have been developed for melanoma and GSK-3 overexpressing tumors and neurodegenerative diseases. Cation lithium is the first inhibitor of GSK-3 to be discovered (49). Although there is no direct therapeutic application for melanoma, Asgari et al. (51) reported that lithium-exposed individuals have a lower incidence and risk of melanoma than unexposed patients. In addition, melanoma patients exposed to lithium have lower melanoma-associated mortality than unexposed individuals (51). Studies on histopathological reflections related to glycogen accumulation that is microscopically represented to have clear cytoplasm and sometimes to accompany cytoplasmic vacuolization and GSK-3 expression levels may be promising for testing new treatment options in melanoma.

Conclusions

On univariate analysis, OS was significantly associated with diagnosis age (grouped by every 3 decades and median age), metastatic site, biopsy type, perivascular pseudorosette, cytoplasmic staining, and nuclear chromatin patterns with H&E and S100 immunohistochemical staining. On the other hand, sex, *BRAF* V600 mutation, melanin pigment, necrosis, mitotic count (divided by 0–6 and more than 6/mm^2), TILs, pleomorphism, cell type, nucleolar prominence, HMB-45, and Melan-A/MART-1 staining were not found to be associated with OS. On the Cox multiple regression model, perivascular pseudorosette, metastatic site, cytoplasmic staining with H&E, and nuclear chromatin patterns remained significantly associated with OS. The main limitations of this study are the limited number of cases, unknown primary sites, and treatment histories.

In conclusion, coincidentally, attention-grabbing perivascular pseudorosette formation in metastatic melanoma was statistically significantly inversely related to OS in both univariate and Cox multiple regression analyses. This may represent a new prognostic histopathologic finding for metastatic melanoma.

References

1. Siegel RL, Miller KD, Fuchs HE, Jemal A. Cancer statistics, 2022. CA Cancer J Clin. 2022;72:7–33.
2. Fisher DE, Bastian BC, editors. Melanoma. New York, NY: Springer; 2019.
3. Elder DE, Bastian BC, Cree IA, Massi D, Scolyer RA. The 2018 World Health Organization classification of cutaneous, mucosal, and uveal melanoma: detailed analysis of 9 distinct subtypes defined by their evolutionary pathway. Arch Pathol Lab Med. 2020;144:500–22.
4. SEER: The Surveillance, Epidemiology, and End Results Program [Internet]. SEER 17 areas (San Francisco, Connecticut, Hawaii, Iowa, New Mexico, Seattle, Utah, Atlanta, San Jose-Monterey, Los Angeles, Alaska Native Registry, Rural Georgia, California excluding SF/SJM/LA, Kentucky, Louisiana, New Jersey, and Georgia excluding ATL/RG) (United states): National Cancer Institute, DCCPS. 2000–2018. [cited 2022 Aug 7] Available from: SEER*Explorer Application (cancer.gov).

5. Belhocine TZ, Scott AM, Even-Sapir E, Urbain JL, Essner R. Role of nuclear medicine in the management of cutaneous malignant melanoma. J Nucl Med. 2006;47:957–67.

6. Crowson AN, Magro CM, Mihm MC. Prognosticators of melanoma, the melanoma report, and the sentinel lymph node. Mod Pathol. 2006;19:S71–87.

7. Xiao Y, Peng S, Hu Y, Zhang J, Cao X. Development and validation of prognostic nomogram in patients with nonmetastatic malignant melanoma: a SEER population-based study. Cancer Med. 2020;9:8562–70.

8. Wiesner T, Kutzner H, Cerroni L, Mihm MC Jr, Busam KJ, Murali R. Genomic aberrations in spitzoid melanocytic tumours and their implications for diagnosis, prognosis and therapy. Pathology. 2016;48:113–31.

9. Cancer Genome Atlas Network. Genomic classification of cutaneous melanoma. Cell. 2015;161:1681–96.

10. Shain AH, Garrido M, Botton T, Talevich E, Yeh I, Sanborn JZ, et al. Exome sequencing of desmoplastic melanoma identifies recurrent NFKBIE promoter mutations and diverse activating mutations in the MAPK pathway. Nat Genet. 2015;47:1194–9.

11. Tsao H, Chin L, Garraway LA, Fisher DE. Melanoma: from mutations to medicine. Genes Dev. 2012;26:1131–55.

12. Elder DE, Massi D, Scolyer RA, Willemze R, editors. WHO classification of skin tumours. 4th ed. Lyon, France: IARC; 2018.

13. Bastian BC, LeBoit PE, Pinkel D. Mutations and copy number increase of HRAS in Spitz nevi with distinctive histopathological features. Am J Pathol. 2000;157:967–72.

14. Yeh I, Botton T, Talevich E, Shain AH, Sparatta AJ, de la Fouchardiere A, et al. Activating MET kinase rearrangements in melanoma and Spitz tumours. Nat Commun. 2015;6:7174.

15. Yeh I, Tee MK, Botton T, Shain AH, Sparatta AJ, Gagnon A, et al. NTRK3 kinase fusions in Spitz tumours. J Pathol. 2016;240:282–90.

16. Wiesner T, He J, Yelensky R, Esteve-Puig R, Botton T, Yeh I, et al. Kinase fusions are frequent in Spitz tumours and spitzoid melanomas. Nat Commun. 2014;5:3116.

17. Curtin JA, Fridlyand J, Kageshita T, Patel HN, Busam KJ, Kutzner H, et al. Distinct sets of genetic alterations in melanoma. N Engl J Med. 2005;353:2135–47.

18. Curtin JA, Busam K, Pinkel D, Bastian BC. Somatic activation of KIT in distinct subtypes of melanoma. J Clin Oncol. 2006;24:4340–6.

19. Furney SJ, Turajlic S, Stamp G, Thomas JM, Hayes A, Strauss D, et al. The mutational burden of acral melanoma revealed by whole-genome sequencing and comparative analysis. Pigment Cell Melanoma Res. 2014;27:835–8.

20. Kaliki S, Shields CL, Shields JA. Uveal melanoma: estimating prognosis. Indian J Ophthalmol. 2015;63:93–102.

21. Esmaeli B, Roberts D, Ross M, Fellman M, Cruz H, Kim SK, et al. Histologic features of conjunctival melanoma predictive of metastasis and death (an American Ophthalmological thesis). Trans Am Ophthalmol Soc. 2012;110:64–73.

22. Esmaeli B, Rubin ML, Xu S, Goepfert RP, Curry JL, Prieto VG, et al. Greater tumor thickness, ulceration, and positive sentinel lymph node are associated with worse prognosis in patients with conjunctival melanoma: implications for future AJCC classifications. Am J Surg Pathol. 2019;43:1701–10.

23. Kestel S, Göçün FPU, Öğüt B, Erdem Ö. Clinicopathologic features and survival outcomes of ocular melanoma: a series of 31 cases from a tertiary university hospital. J Pathol Transl Med. 2022;56:187–98.

24. Amin MB, Edge SB, Greene FL, Byrd DR, Brookland RK, Washington MK, et al., editors. AJCC cancer staging manual. 8th ed. New York: Springer; 2017.

25. Rambhia PH, Scott JF, Vyas R, Gerstenblith MR. Genitourinary melanoma. In: Scott JF, Gerstenblith MR, editors. Noncutaneous melanoma [Internet]. Brisbane (Australia): Codon Publications; 2018 Mar. Chapter 5.

26. Sandru A, Voinea S, Panaitescu E, Blidaru A. Survival rates of patients with metastatic malignant melanoma. J Med Life. 2014;7:572–6.

27. Tas F, Erturk K. Early and late relapses of cutaneous melanoma patients. Postgrad Med. 2019;131:207–11.

28. Gajdos C, McCarter MD. Debulking surgery in advanced melanoma. Expert Rev Anticancer Ther. 2011;11:1703–12.

29. Banerjee SS, Harris M. Morphological and immunophenotypic variations in malignant melanoma. Histopathology. 2000;36:387–402.

30. Upadhyay Baskota S, Monaco SE, Xing J, Pantanowitz L. Peritheliomatous pattern: a diagnostic clue for diagnosing metastatic melanoma in cytology. Cancer Cytopathol. 2020;128:260–8.

31. Pföhler C, Thirkill CE, Tilgen W. Rosette formation in melanoma: more frequent than suspected? Am J Dermatopathol. 2003;25:360–1.

32. Alonso S, Rodríguez-Peralto JL, Ballestín C, Ortiz P. Metastatic malignant melanoma with Homer-Wright rosettes mimicking a neuroblastic tumor. An unusual morphological manifestation. Virchows Arch. 2003;443:108–10.

33. Falconieri G, Luzar B, Angione V, DeMaglio G, Pizzolitto S. Primary cutaneous nevoid melanoma with Homer-Wright rosettes: a hitherto unrecognized variant with immunohistochemical and ultrastructural study. Am J Dermatopathol. 2010;32:606–9.

34. Miller K, Hall RC, Brenn T. Spitz nevus with Homer-Wright rosette-like structures. Am J Dermatopathol. 2012;34:457–9.

35. Ishida M, Iwai M, Yoshida K, Kagotani A, Okabe H. A distinct histopathological variant of a malignant melanoma with perivascular pseudorosettes: a case report. Oncol Lett. 2013;6:673–5.

36. Orgaz JL, Sanz-Moreno V. Emerging molecular targets in melanoma invasion and metastasis. Pigment Cell Melanoma Res. 2013;26:39–57.

37. Fukunaga-Kalabis M, Roesch A, Herlyn M. From cancer stem cells to tumor maintenance in melanoma. J Invest Dermatol. 2011;131:1600–4.

38. Bailey CM, Morrison JA, Kulesa PM. Melanoma revives an embryonic migration program to promote plasticity and invasion. Pigment Cell Melanoma Res. 2012;25:573–83.

39. Sleeman JP, Cady B, Pantel K. The connectivity of lymphogenous and hematogenous tumor cell dissemination: biological insights and clinical implications. Clin Exp Metastasis. 2012;29:737–46.

40. Lugassy C, Barnhill RL, Christensen L. Melanoma and extravascular migratory metastasis. J Cutan Pathol. 2000;27:481.

41. Lugassy C, Zadran S, Bentolila LA, Wadehra M, Prakash R, Carmichael ST, et al. Angiotropism, pericytic mimicry and extravascular migratory metastasis in melanoma: an alternative to intravascular cancer dissemination. Cancer Microenviron. 2014;7:139–52.

42. Lugassy C, Barnhill RL. Angiotropic malignant melanoma and extravascular migratory metastasis: description of 36 cases with emphasis on a new mechanism of tumour spread. Pathology. 2004;36:485–90.

43. Barnhill RL, Dy K, Lugassy C. Angiotropism in cutaneous melanoma: a prognostic factor strongly predicting risk for metastasis. J Invest Dermatol. 2002;119:705–6.

44. Van Es SL, Colman M, Thompson JF, McCarthy SW, Scolyer RA. Angiotropism is an independent predictor of local recurrence and in-transit metastasis in primary cutaneous melanoma. Am J Surg Pathol. 2008;32:1396–403.

45. Wilmott J, Haydu L, Bagot M, Zhang Y, Jakrot V, McCarthy S, et al. Angiotropism is an independent predictor of microscopic satellites in primary cutaneous melanoma. Histopathology. 2012;61:889–98.

46. Fornabaio G, Barnhill RL, Lugassy C, Bentolila LA, Cassoux N, Roman-Roman S, et al. Angiotropism and extravascular migratory metastasis in cutaneous and uveal melanoma progression in a zebrafish model. Sci Rep. 2018;8:10448.

47. Macák J, Krc I, Elleder M, Lukás Z. Clear cell melanoma of the skin with regressive changes. Histopathology. 1991;18:276–7.

48. Nowak MA, Fatteh SM, Campbell TE. Glycogen-rich malignant melanomas and glycogen-rich balloon cell malignant melanomas: frequency and pattern of PAS positivity in primary and metastatic melanomas. Arch Pathol Lab Med. 1998;122:353–60.

49. Mancinelli R, Carpino G, Petrungaro S, Mammola CL, Tomaipitinca L, Filippini A, et al. Multifaceted roles of GSK-3 in cancer and autophagy-related diseases. Oxid Med Cell Longev. 2017;2017:4629495.

50. Kubic JD, Mascarenhas JB, Iizuka T, Wolfgeher D, Lang D. GSK-3 promotes cell survival, growth, and PAX3 levels in human melanoma cells. Mol Cancer Res. 2012;10:1065–76.

51. Asgari MM, Chien AJ, Tsai AL, Fireman B, Quesenberry CP Jr. Association between lithium use and melanoma risk and mortality: a population-based study. J Invest Dermatol. 2017;137:2087–91.